Römer, G.R.B.E.; Arnaldo Del Cerro, D.; Pohl, R.; Chang, B.; Liimatainen, V.; Zhou, Q.; Huis In‘t Veld, A.J.

Picosecond laser machining of metallic and polymer substrates for fluidic driven self-alignment

Published in:
Physics Procedia

DOI:
10.1016/j.phpro.2012.10.082

Published: 01/01/2012

Document Version
Publisher's PDF, also known as Version of record

Please cite the original version:
Römer, G. R. B. E., Arnaldo Del Cerro, D., Pohl, R., Chang, B., Liimatainen, V., Zhou, Q., & Huis In‘t Veld, A. J. (2012). Picosecond laser machining of metallic and polymer substrates for fluidic driven self-alignment. *Physics Procedia*, *30*, 628–635. https://doi.org/10.1016/j.phpro.2012.10.082

Available online at www.sciencedirect.com

SciVerse ScienceDirect

Physics Procedia 39 (2012) 628 – 635

Physics Procedia

LANE 2012

Picosecond laser machining of metallic and polymer substrates for fluidic driven self-alignment

G.R.B.E. Römer[a,*], D. Arnaldo del Cerro[a], R. Pohl[a], B. Chang[b], V. Liimatainen[b], Q. Zhou[b], A.J. Huis in 't Veld[a,c]

[a]*University of Twente, Chair of Applied Laser Technology, Drienerlolaan 5, Enschede, 7522N , The Netherlands*
[b]*AALTO University, Electrical Engineering, Dept. Automation and Systems Technology, Aalto, 00076, Finland*
[c]*TNO Mechatronics, Mechanics and Materials, De Rondom 1, Eindhoven, 5600 HE, The Netherlands*

Abstract

Fluidic self-alignment of micro-components relies on creating a receptor site that is able to confine a liquid droplet. When a micro-component is brought in contact with the droplet, capillary forces move the component to its final position. A method to stop the advancing of a liquid from a receptor site, consists of creating geometrical features, such as edges around the site. A picosecond pulsed laser source was used to create suitable edges in a metallic and a polyimide substrate. Subsequently, the self-alignment capabilities of these sites were tested. The receptor sites in polyimide showed the highest success rate.

Keywords: Laser; Ultra short pulse; fluidic self-alignment

1. Introduction

Fluid driven self-alignment is a low cost alternative to fast, but relatively inaccurate robotic pick-and-place assembly of micro-fabricated components [1,2], see Fig. 1. The fluidic self-alignment technique relies on a hydrophobic-hydrophilic pattern on the surface of the receiving substrate, which confines the fluid to a receptor site (Fig. 1b). When a micro-component, with dimensions in the order of 100×100 μm^2, is "dropped" on the fluid (Fig. 1c and 1d), capillary forces drive the alignment of the part to the receptor site (Fig. 1e). When the shape, as well as the relative wetting properties of the receptor site, as well as of the part, are optimized, this self-alignment technique allows for accurate positioning (about ±2μm) of the

* Corresponding author. Tel.: +31-53-4892519 ; fax: +31-53-4893631 .
E-mail address: g.r.b.e.romer@utwente.nl .

 doi:10.1016/j.phpro.2012.10.082

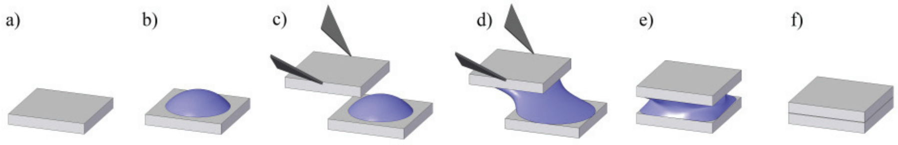

Fig. 1. Fluid driven self-alignment [2]: (a) receptor site; (b) a droplet of a liquid is dispensed on the receptor site; (c) a gripper approaches the site with a part; (d) the part contacts with the droplet; (e) the gripper releases the part and the capillary force aligns the parts; (f) the liquid between the two parts evaporates, which leaves the two parts aligned

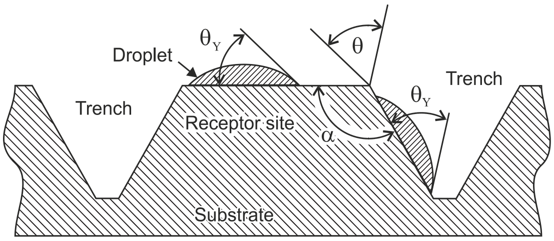

Fig. 2. An receptor site can be created by removing material (by laser ablation) from the tracks of a laser path that follows the perimeter of the site. The sharper angle α of the edge of the resulting trench, the more it will impede the liquid front from crossing the edge

part to the receptor site. Orientation accuracies of the part relative to the receptor site of typically ±0.5º have been reported [3]. Moreover, it was shown, that capillary forces can overcome initial positioning errors (Fig. 1d) of up to 180μm in the case of a part of 300×300μm^2 [3].

Ultra Short Pulse Laser (USPL) sources, with pulse durations in picosecond (ps) regime and smaller, have proven to be versatile tools for introducing functional features in surfaces at a micrometric and even at a sub-wavelength scale. Being able to control the surface topography at this level allows to change the wetting behaviour (hydrophobicity and hydrophilicity) of a great number of materials. As such, micromachining with USPL sources allows for fast, flexible and accurate control of the surface topography, hence of the wetting properties of surfaces. This paper studies the use of a ps laser source for the fabrication of hydrophobic-hydrophilic patterns on a substrate to allow for fluid driven self-alignment.

The ability of a receptor site to pin/confine the droplet depends on three key factors:

i. the chemical composition of the surface of the substrate, and
ii. its topography, which can be subdivided into two factors related to:
    a. roughness or texture, of the surface, and
    b. geometrical features, such as edges, that are able to stop the advancing of a liquid front.

Factor ii.b can be efficiently and effectively exploited when applying an USPL source. That is, well-defined edges around the receptor site can be created by selectively removing material from the perimeter of the receptor site, by laser ablation, see Fig. 2. The edges of the tracks will provide a location for the pining of the liquid-solid-vapour interface of a droplet. It has been shown [4,5] that the sharper the angle α [deg] of an edge the more it will impede the liquid front from crossing the modified perimeter, see Fig. 2. The latter is described by Gibbs inequality $\theta_Y < \theta < (180\text{-}\alpha) + \theta_Y$, where θ_Y [deg] is Young's equilibrium contact angle, which a droplet adopts when in contact with a flat/smooth surface [4]. It follows from this inequality that, a large local contact angle θ [deg] will be formed, before a liquid front overflows an edge/obstacle with a small edge angle α. Sharp edges (with small values of α) can be accurately machined by a proper selection of the laser processing parameters. This approach, exploiting factor ii.b to pin the liquid, is suitable for both hydrophobic and hydrophilic substrates and is therefore, more flexible than the alternative approaches i. and ii.a, listed above.

2. Materials and experimental setup

Laser machining of two types of substrates, common in the semi-conductor industry, were studied. First a copper base material with thin top metal sandwich finish, which is a popular leadframe in the electronics industry. It is composed of a copper foil (bulk) with, on top, a standard roughened PrePlated Finish (PPF), consisting of a sandwich of thin layers of Gold, Paladium and Nickel of about 1.5 to 2µm in total. The second substrate studied was polyimide (PI) foil with a thickness of 25±2 µm. To allow easy handling, this foil was fixed on a copper sheet of about 230 µm thickness.

An Yb:YAG laser source, type TRUMICRO 5050 of TRUMPF, with pulse duration of 6.7 ps and with a central wavelength of 1030nm (IR) was used for generation of the laser pulses. A Third Harmonic Generation (THG) unit was applied to convert the central wavelength to 343nm (UV), as the absorption of laser energy of the substrate at this wavelength is higher than at IR. The beam shows a nearly Gaussian power density profile (M^2<1.3). The radiation was linearly polarized. Manipulation of the beam over the samples was accomplished by a two mirror Galvano-scanner system, type INTELLISCAN14 of SCANLAB. A telecentric 100 mm f-θ-lens, type RONAR of LINOS focused the beam. The substrates were irradiated at normal incidence at environmental conditions. The pulse frequency (or pulse repetition rate) f_p [Hz] of the laser source, as well as the beam diameter d [m] of the focal spot, and the velocity v [m/s] of the laser spot relative to the substrate, determine the spatial pulse-to-pulse overlap (*OL*) of subsequent laser pulses, and is defined here as $OL = [1\text{-}v/(d{\cdot}f_p)]\times 100\%$.

The surface topography of the machined surfaces was analyzed by a Confocal Laser Scanning Microscope (CLSM), type VK-9700, of KEYENCE, and a Scanning Electron Microscope (SEM), type JCM NEOSCOPE 5000 of JEOL. A custom build micro-assembly system was used to carry out self-alignment tests [3]. This system includes a robotic microgripper, two microscopes, three motorized stages and a droplet dispenser.

3. Experimental results and discussion

3.1. Results on copper base material with PPF finish

Measurements, using the CLSM, showed that the surface roughness of the unmachined leadframe was R_a≈1.5µm. Note that this roughness is about as large as the thickness of the PFF layer. Next, the ablation threshold was determined using the so-called D^2-method [6]. This method also allows to determine the diameter of the laser spot, which was found equal 15.6 µm. The ablation threshold was found to be 0.11 J/cm^2, which corresponds to a pulse energy of 0.10 µJ.

Next, laser machining conditions were determined to create trenches with targeted depths of 0.5 µm, 1.0 µm, 2.0 µm and 5.0 µm. To that end, first single lines were machined at pulse energies E_p [J] ranging from 0.05µJ and 0.25µJ and at number of overscans N ranging from 10 to 1000. To study the effect of pulse-to-pulse overlap (OL), the beam velocity v was varied between 0.2 m/s and 0.4 m/s. It was verified experimentally that, at the fixed pulse frequency of 400kHz, the laser radiation of a pulse did not intervene with the plasma generated by ablation induced by a previous pulse (plasma shielding). Nor were

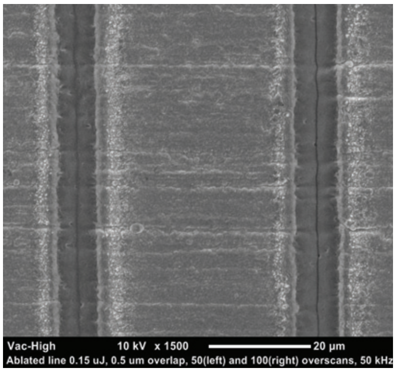

(a) SEM image, Scale bar 20µm

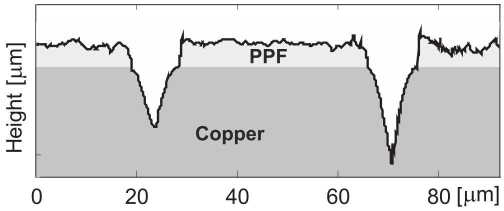

(b) CLSM cross-section.

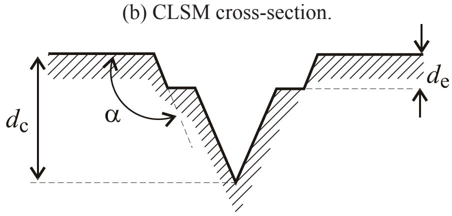

(c) Definition of track edge depth d_e, edge angle α and track depth d_c

Fig.3. (a) SEM and (b) CLSM images of two laser tracks/lines; E_p=0.15 µJ, N=50 (left), N=100 (right), and (c) definitions of geometry

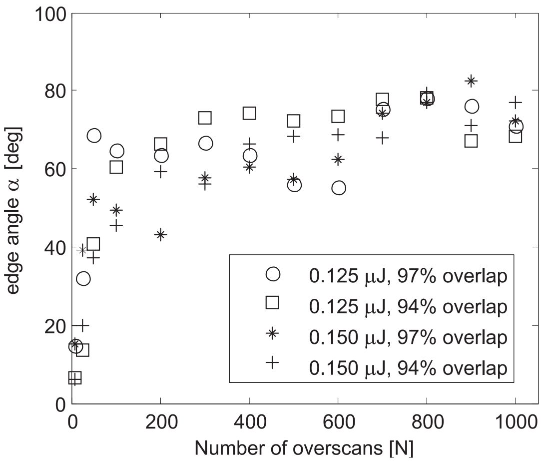

Fig. 4. Measured edge angle as a function of E_p, OL and N

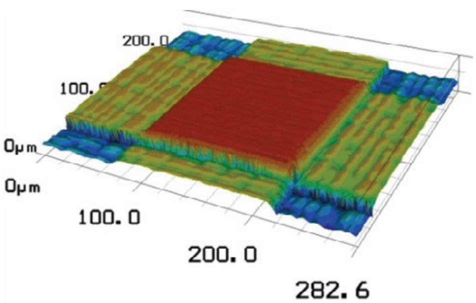

Fig. 5. CLSM image of a receptor site with sharp edges, created with processing conditions of parameter set 4

signs of temperature build up in the substrate, due to accumulation of heat, observed. Fig. 3a shows a SEM image of two typical single laser tracks. Fig. 3b shows a CLSM cross-section of those tracks. Evident in Fig. 3a are horizontal scratches, probably caused by polishing in the production of the leadframe, leading to the aforementioned surface roughness.

As can be observed from Fig. 3b, the cross section clearly shows a sharp change in ablated height d_e at the edges of the ablated line. It was concluded that this sharp change in height is caused by the removal/ablation of the PPF layer, because d_e was found to show a maximum of about 1.5 to 2.5µm. As the liquid confinement capability of a receptor site depends on the geometrical angle of the edges of the site, the edge angle α [deg] (Fig. 3c) of the laser generated tracks were measured by CLSM, see Fig. 4. It can be observed that, for a fixed pulse energy, the edge angle increases from about 10° to about 65°, when increasing overscans from N=10 to 100. At higher number of overscans, so N>100, the edge angle gradually increases towards 90°. From these results, four processing conditions were selected to create trenches with the targeted depths, see Table 1.

Table 1. Processing conditions to create trenches and measured geometrical properties of the trenches around the receptor sites created with these conditions

Parameter set	Targeted depth [μm]	E_p [μJ]	Pulse-to-pulse distance [μm]	N [#]	f_p [Hz]	Measured depth [μm]	Measured edge angle α [deg]
1	0.5	0.1	1	25	400	0.546±0.115	153.6±8.1
2	1	0.125	1	50	400	1.311±0.595	141.9±22.9
3	2	0.225	0.5	10	50	2.023±0.306	160.7±8.1
4	5	0.225	0.5	50	50	8.408±2.204	134.2±3.2

To create trenches wider than the width of a single ablated track, several parallel laser tracks were machined next to each other, to create an "area" of ablated material. Striving for a flat bottom of the trench, the hatch distance between tracks was chosen as one third of the width of a single laser track. Targeted trench width is about 100μm, to ensure that the droplet used for self-alignment experiments will not be affected by the width of the trench. Next, every area was rescanned N times (overscans). By creating four of these areas in a square pattern, square receptor sites were obtained, see Fig. 5. Note that, the horizontal and vertical trenches overlap in the corners resulting in $2N$ overscans at those locations. The measured trench depth and edge angle α around the receptor site are listed in the last two columns of Table 1.

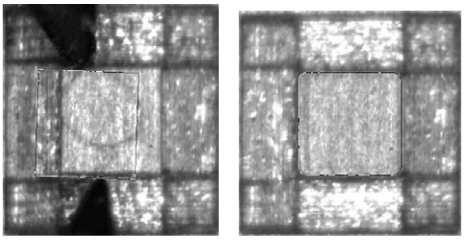

Fig. 6. An example of a successful self-alignment test with a 200×200μm SU-8 chip, where the edges of the chip have been high-lighted. Shown are: (a) chip at releasing position, see Fig. 1e; (b) final position after successful self-alignment, see Fig. 1f

Self-alignment tests, using the custom build micro-assembly system (section 2), were performed on receptor sites each with different edge angles. See Fig. 6 for an example. To that end, 50 μm thick SU-8 chips of 200×200μm^2 were used as test parts to be aligned. The polymer SU-8 is an epoxy-based photoresist, which was chosen here for its transparency to visual light. The latter allows access of the position accuracy of the SU-8 chip the receptor site after alignment. The experiment comprised of the following five steps: (*i*) the chip is moved to a predefined releasing position near the receptor site, (*ii*) a droplet of distilled water is dispensed on the site, (*iii*) the chip is released on the droplet, (*iv*) the chip aligns itself to the site, (*v*) after a few seconds the water vaporizes, leaving the chip on the receptor site. The performance self-alignment of the SU-8 chip was verified 6 times for each site. It was found that, only receptor sites with a trench depth of more than 2 μm showed a 100% success rate of self-alignment of the chip. The results suggest that the height of the patterns is critical for self-alignment. However, it should be noted that the initial surface roughness of 1.5μm will most probably have a strong effect on the success rate. To confirm this, polyimide was processed as this substrate showed a much lower initial surface roughness.

3.2. Results on polyimide (PI)

Measurements, using the CLSM, showed that the surface roughness of the PI, prior to laser machining, was R_a ≈0.04µm. Using the D^2-method, the ablation threshold was found to equal 0.06 J/cm^2. Next, laser machining conditions were experimentally determined to create trenches in the substrate. The velocity of the focal spot relative to the substrate was fixed to v=0.4 m/s, and the pulse frequency to f_p=400 kHz. With the beam diameter of 15.6 µm, this implies an overlap of OL=97%. The pulse energy E_p was varied between 0.25 and 1 µJ, and the number of overscans N was varied from N=1 to 25 to study the effect of these parameters on the geometry (width, depth and edge angle) of the trenches. It was found from CLSM that, the trench width (ranging from about 15 µm to 23 µm) and depth (ranging from 1 µm to 20 µm) increase more or less linearly with the number of overscans and the pulse energy.

Fig. 7 shows that the edge angle α decreases with increasing number of overscans and increasing pulse energy. Careful analysis of the dependency of the edge angle on the number of overscans at a pulse energy of 1 µJ, shows a discontinuous drop in edge angle from about α=140º to 95º, when the number of overscans is increased from N=3 to 4. To explain this result, cross sections of trenches, at a pulse energy of 1µJ, as a function of number of overscans were derived from CLSM measurement, see Fig. 8. As can be observed from these cross sections, the edges are "smooth" for overscans up to N=3. For N=4 and 5 the edges of the trench show a characteristic "dent" and "hump". The humps show steep edge angles, as small as 92º, which provide a suitable geometrical feature to stop the advancing of the liquid [5]. Similar dents and humps have been previously reported in nanosecond and picosecond UV-laser ablation of PI [7-9]. These studies attribute the humps to a volume increase due to two mechanisms: amorphization of crystalline domains and fragmentation of polymer chains. It is worthy to mention that with polymers, hydrodynamic motions are hindered because of high viscosity of melts [10]. And that, with thermostable polymers as polyimide, ablation craters do not exhibit residues of melting [11].

Dent formation is explained by relaxation of preexistent internal stresses. This mechanism would cause shrinking of the PI. According to the single pulse experiments of Piglmayer et al. [8], dent and hump formation can occur when the (local) laser fluence near or just below the ablation threshold of the material. Indeed, it was confirmed that the humps and dents in Fig. 8 occur near the ablation threshold of the applied Gaussian fluence profile. It should be noted however, that the features in Fig. 8 appear only after exposing PI to multiple overlapping pulses, in contrast to the single shot experiments by Piglmayer

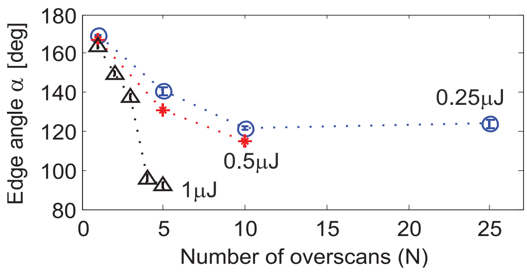

Fig. 7. Edge angle, obtained by CLSM, of single laser tracks (trenches) in PI as a function of number of overscans N and pulse energy. Each data point is an average of 4 measurements

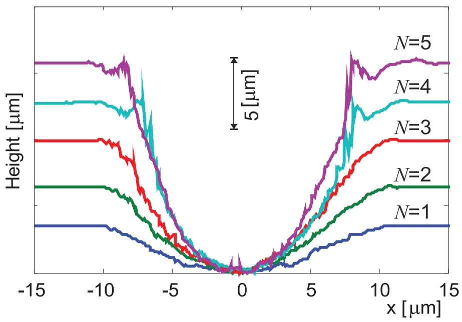

Fig. 8. Cross sections, obtained by CLSM, of single laser tracks (trenches) in PI as a function of number of overscans N at a pulse energy of 1µJ, v=0.4 m/s, f_p=400 kHz. Each cross section is an average of 4 measurements

et al. Further, Himmelbauer et al. [7] as well as Piglmayer et al. applied relatively long pulse durations of 140 ns up to 50 ms, when compared to the pulse duration of 6.7 ps which was applied in this study. An incubation effect, responsible for the growth of dents and humps after successive 6.7 ps laser pulses, might provide an explanation for the surface features shown in Fig. 8. Further research would be required to confirm this. Anyhow, the humps and dents are constant along edge of the trench and display sharp edged sides. Those sharp edges provide an excellent pinning location for an advancing front of liquid of receptor sites.

Next, receptor sites of 200×200 μm^2 were created in the PI substrate, using processing conditions listed in the caption of Fig. 8. In addition to those conditions, receptor sites were created additional overscans equal to N=6 and 7. The edge angle of the trench surrounding the sites were measured from CLSM measurements, see Fig. 9. It was made sure that the edge angle of the hump (only) was determined, as it is this part of the edge which will stop a fluid from advancing off the site.

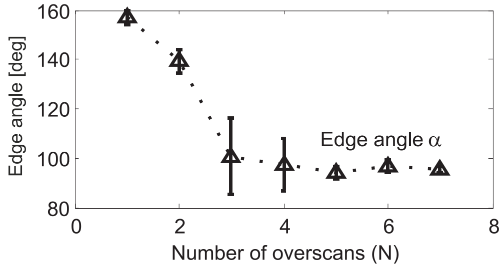

Fig. 9. Edge angle α of trenches surround receptor sites in PI, as a function of number of overscans N. E_p = 1μJ, v=0.4 m/s f_p=400 kHz. Each data point is an average of 8 measurements

Self-alignment tests were performed on these receptor sites. The performance of self-alignment of the SU-8 chip was verified 11 times for each site. All sites showed a 100% success rate of self-alignment, except the sites with the largest edge angles of 156º and 139.4º, which showed a success rate of only 0% and 54.6% respectively. Failing self-alignment on these sites could be attributed to water overflowing the receptor site before, or during, self-alignment. In the case of the site with edge angle of 156º, the droplets were found to overflow the edge before the chip is dropped on the water. This can be attributed to the fact that, the water droplets are shot at an angle on receptor site. The latter implies that the momentum of the injected droplet might drive the fluid off the site into the trench. In the case of sites, with an edge angle of 139.4º, the advancement of the droplet was successfully stopped by the edges of the receptor site in only some of the experiments. It was found that the receptor sites, with humped edges, showed a 100 % success rate. The final positional and rotational errors of the chip relative to the site were found to equal 0.25±0.86 μm and 0.35±1.22 º respectively. It should be noted however that the resolution of the camera was too low to allow (more) accurate measurements

4. Conclusions

A 6.7 ps laser source, operating at 343nm wavelength, 400kHz, with a focus diameter of 15.6 μm was used to create receptor sites for fluidic self-alignment. Sites of 200×200 μm^2 were created in a metallic leadframe with a PrePlated Finish, as well as in a polyimide foil. Spreading of liquid from these sites were shown to be stopped by a sharp geometrical edge around the site created by laser ablation. Trenches around sites in the leadframe were created at pulse energies ranging from 0.1 μJ to 0.225 μJ, spatial pulse-to-pulse overlap ranging from 94% to 97%, and number of overscans ranging from 10 to 50.

Trenches around sites in the leadframe were created at a pulse energy of 0.1 μJ to 0.225 μJ, pulse overlap of 97%, and number of overscans ranging from 1 to 7.

It was found that the success rates of self-alignment of 200×200 μm^2 SU8 chips to the receptor sites in the leadframe is high only if the height of the receptor site is well over the initial surface roughness of the substrate. Near the edges of the sites in polyimide, characteristic "dents" and "humps" were found showing steep edge angles up to about 95º. These edge features provide a suitable geometrical feature to stop the advancing of the liquid which drives self-alignment. It was found, that the success rates of self-alignment of parts is 100% if the angle of the edges of the receptor site are sharp, due to these dents and humps. The final positional and rotational errors of the chip were found equal 0.25±0.86 μm and 0.35±1.22º respectively.

Acknowledgements

The authors would like to acknowledge the financial support of the European Union 7th Framework Programme FP7-2010-NMP-ICT-FoF under Grant Agreement No. 260079 - Efficient and Precise 3D Integration of Heterogeneous Microsystems from Fabrication to Assembly (http://www.fab2asm.eu).

References

[1] S.H. Liang, X. Xiong, K.F. Böhringer, Towards optimal designs for self-alignment in surface tension driven micro-assembly, Proceedings of the 17th IEEE In-ternational Conference on. (MEMS) Micro Electro Mechanical Systems, pp. 9-12, (2004).

[2] V. Sariola, Mirva Jääskeläinen and Q. Zhou, Hybrid Microassembly Combining Robotics and Water Droplet Self-Alignment, IEEE transactions on robotics, 26(6) (2010).

[3] V. Sariola, Droplet Self-alignment: High-precision robotic micorassmebly and self-assembly. PhD-thesis. Aalto University, School of Electrical Engineering, Department of Automation and Systems Technology (2012).

[4] J.W. Gibbs. Scientific Papers Vol. 1, Longmans, London (1906), p. 326 (Dover reprint, New York, 1961).

[5] J. F. Oliver, C. Huh, S. G. Mason, Resistance to spreading of liquids by sharp edges, Journal of Colloid and Interface Science 59 (3) (1977) 568–581.

[6] J. Bonse, J.M. Wrobel, J. Krüger, and W. Kautek. Ultrashort-pulse laser ablation of indium phosphide in air. Applied Physics A, 72(1):89–94, 2001.

[7] M. Himmelbauer, E. Arenholz, D. Bäuerle, and K. Schilcher. UV-laser-induced surface topology changes in polyimide. Applied Physics A, 63:337–339 (1996).

[8] K. Piglmayer, E. Arenholz, C. Ortwein, N. Arnold, and D. Bäuerle. Single-pulse ultraviolet laser-induced surface modification and ablation of polyimide. Applied Physics Letters, 73:847–849 (1998).

[9] A.A. Serafetinides, C.D. Skordoulis, M.I. Makropoulou, and A.K. Kar. Picosecond and subpicosecond visible laser ablation of optically transparent polymers. Applied Surface Sciences, 135:276–284 (1998).

[10] N. Bityurin, B. S. Luk'yanchuk, M. H. Hong, and T. C. Chong. Models for Laser Ablation of Polymers. Chemical Reviews, 103(2): 519-552 (2003).

[11] D. Bäuerle, Laser Processing and Chemistry, 4th edition, Springer, Heidelberg (2011).